

Coherent Association of Single Molecules from Single Atoms

A DISSERTATION PRESENTED
BY
YICHAO YU
TO
THE DEPARTMENT OF PHYSICS

IN PARTIAL FULFILLMENT OF THE REQUIREMENTS
FOR THE DEGREE OF
DOCTOR OF PHILOSOPHY
IN THE SUBJECT OF
PHYSICS

HARVARD UNIVERSITY
CAMBRIDGE, MASSACHUSETTS
MARCH 2021

©2021 – YICHAO YU
ALL RIGHTS RESERVED.

Thesis advisor: Professor Kang-Kuen Ni

Yichao Yu

Coherent Association of Single Molecules from Single Atoms

ABSTRACT

Contents

o	INTRODUCTION	1
1	APPARATUS	2
1.1	Cooling and Optical Pumping Beams	2
1.2	Tweezer and Imaging	3
1.3	Molecular Raman Frequency Generation	3
2	COMPUTER CONTROL OF THE EXPERIMENT	4
2.1	Overall Structure	4
2.2	Frontend	4
2.3	Backends	5
2.4	Automation of Scan	5
2.5	Summary and Outlook	5
3	RAMAN SIDEBAND COOLING	6
3.1	Introduction	6
3.2	Theory	6
3.3	Setup	7
3.4	Challenge with Large Lamb-Dicke Parameter	7
3.5	Solution: High Order Sidebands	7
3.6	Solution: Simulation Based Optimization	9
3.7	Cooling Performance	9
4	INTERACTION OF SINGLE ATOMS	13
4.1	Scattering Length	13
4.2	Energy Levels of Two Interacting Atoms in an Anisotropic Trap	13
4.3	Interaction Shift Spectroscopy	14
4.4	Summary and Outlook	14
5	PHOTOASSOCIATION OF SINGLE ATOMS	15
5.1	Energy Levels	15
5.2	Effect of the Trap	15
5.3	Photoassociation Spectroscopy	16
6	TWO-PHOTON SPECTROSCOPY OF NACs GROUND STATE	17

6.1	Introduction	18
6.2	Energy Level Structure for NaCs Ground State	18
6.3	Raman Resonance on $v'' = -1$, $N = 0$ Ground State	18
6.4	Raman Resonance on $v'' = -1$, $N = 2$ Ground State	18
7	COHERENT OPTICAL CREATION OF NaCs MOLECULE	19
7.1	Introduction	20
7.2	Raman Transfer Efficiency Model	20
7.3	Excited State Selection	20
7.4	Ground States Selection	20
7.5	Raman Transition Results	20
8	CONCLUSION	21
	APPENDIX A COMPUTER CONTROL APPENDIX	22
	APPENDIX B RAMAN SIDEBAND COOLING APPENDIX	23
	REFERENCES	30

Acknowledgments

,

0

Introduction

1

Apparatus

1.1 COOLING AND OPTICAL PUMPING BEAMS

(MOT, OP, fiber back reflection)

(Mention Na Raman beam to be covered in later chapter?)

1.2 TWEEZER AND IMAGING

1.3 MOLECULAR RAMAN FREQUENCY GENERATION

(beam path, calibration)

2

Computer Control of the Experiment

2.1 OVERALL STRUCTURE

2.2 FRONTEND

(Abstraction) (Backward compatibility) (Flexibility) (Text based/version control friendly)

2.3 BACKENDS

(communication protocol) (IR)

2.3.1 FPGA BACKEND

(clock generation) (pulse merging) (compression)

2.3.2 NIDAQ BACKEND

(Variable clock)

2.3.3 USRP BACKEND

(SIMD)

2.4 AUTOMATION OF SCAN

(Scan requirement) (Combination of scans) (Scope/nested structure)

2.5 SUMMARY AND OUTLOOK

(new backend/SPCM) (native code generation, auto vectorization) (dynamic logic and dependency tracking/optimization)

3

Raman Sideband Cooling

3.1 INTRODUCTION

3.2 THEORY

3.1



Figure 3.1: Single Na atom Raman sideband cooling scheme. The Raman transitions between $|2, 2; n\rangle$ and $|1, 1; n + \Delta n\rangle$ have a one-photon detuning $\Delta = 75$ GHz below the $3^2S_{1/2}$ to $3^2P_{3/2}$ transition. Two-photon detuning, δ , is defined relative to the $\Delta n = 0$ carrier transition. For optical pumping, we use two σ^+ polarized transitions, one to pump the atom state out of $|1, 1\rangle$ via $3^2P_{3/2}$ and one to pump atoms out of $|2, 1\rangle$ via $3^2P_{1/2}$ to minimize heating of the $|2, 2\rangle$ state.

3.3 SETUP

3.2

3.4 CHALLENGE WITH LARGE LAMB-DICKE PARAMETER

3.3

3.5 SOLUTION: HIGH ORDER SIDEBANDS

3.4

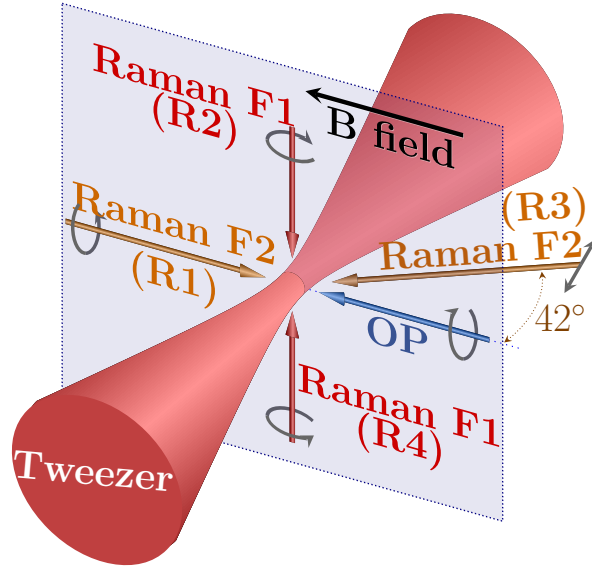


Figure 3.2: Geometry and polarizations of the Raman and optical pumping beams relative to the optical tweezer and bias magnetic field. Raman beams R1 and R4 address the radial x -mode. R1 and R2 address the radial y -mode. R3 and R4 address the axial z -mode, where the beams also couple to radial motion, but this coupling can be neglected when the atoms is cooled to the ground state of motion.

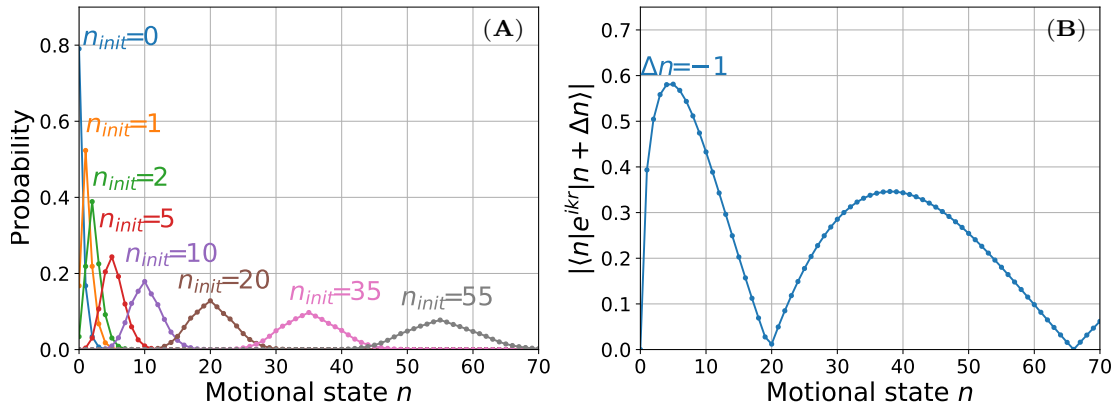


Figure 3.3: Optical pumping motional-state redistribution and Raman coupling for large LD parameters for the axial direction (z). The range plotted covers 95% of the initial thermal distribution. (A) Motional state distribution after one OP cycle for different initial states motion, n_{init} . Due to photon-recoil and the large LD parameter, $\eta_z^{\text{OP}} = 0.55$, there is a high probability of n changing. (B) Matrix elements for Raman transition on the first order cooling sideband deviate from \sqrt{n} scaling with multiple minima.

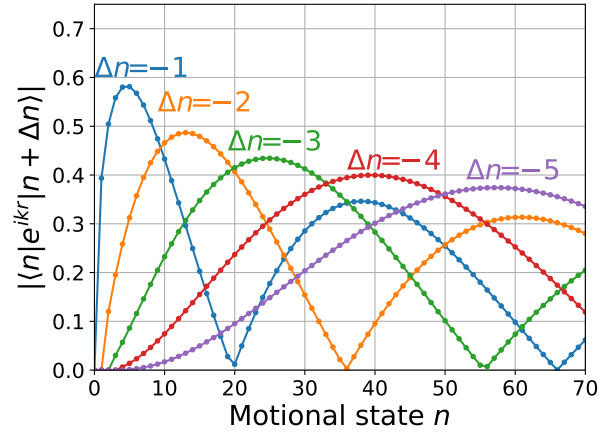


Figure 3.4: Matrix elements for Raman transition including high order sidebands. During cooling, we utilize the fact that high motional states couple most effectively to sidebands with large $|\Delta n|$ in order to overcome the issue with variation and dead zone in the coupling strengths.

3.6 SOLUTION: SIMULATION BASED OPTIMIZATION

3.5

3.7 COOLING PERFORMANCE

3.6 3.7

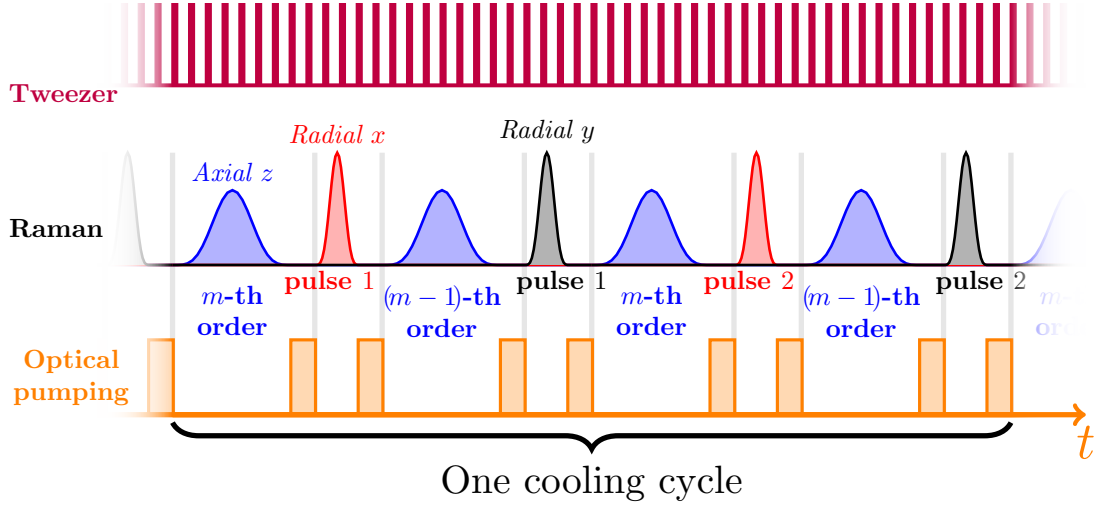


Figure 3.5: Schematic of the cooling pulse sequence. The tweezer is strobed at 3 MHz to reduce light shifts during optical pumping. Each cooling cycle consists of 8 sideband pulses. The four axial pulses address two sideband orders. The two pulses in each radial direction either address $\Delta n = -2$ and $\Delta n = -1$ or have different durations to drive $\Delta n = -1$, at the end of the cooling sequence when most of the population is below $n = 3$. The Raman cooling and spectroscopy pulses have Blackman envelopes to reduce off-resonant coupling, while the measurement Rabi pulses in Fig. 3.7 have square envelopes to simplify analysis.

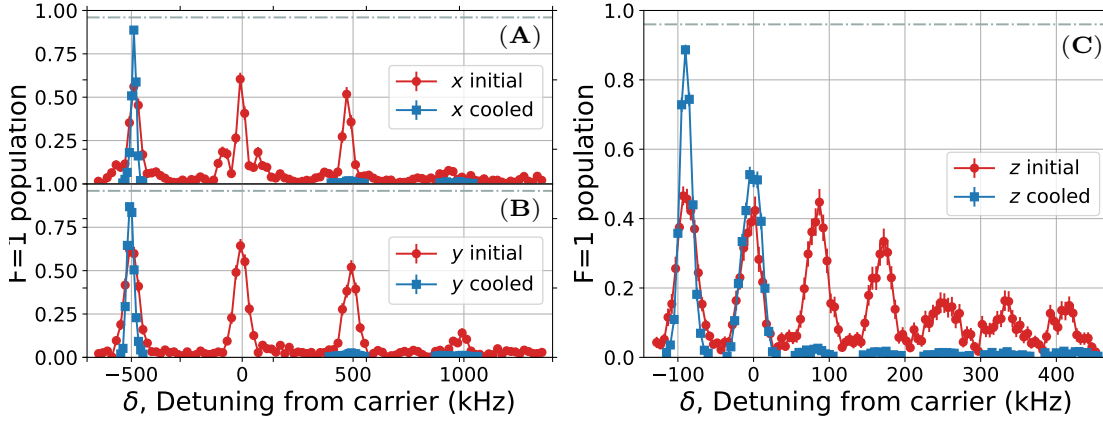


Figure 3.6: Raman sideband spectra for (A) x , (B) y , (C) z axis before (red circle) and after (blue square) applying Raman sideband cooling sequence. The height of the cooling sidebands (positive detuning) are strongly suppressed after cooling which suggests most of the atoms are cooled to the motional ground state in the trap.

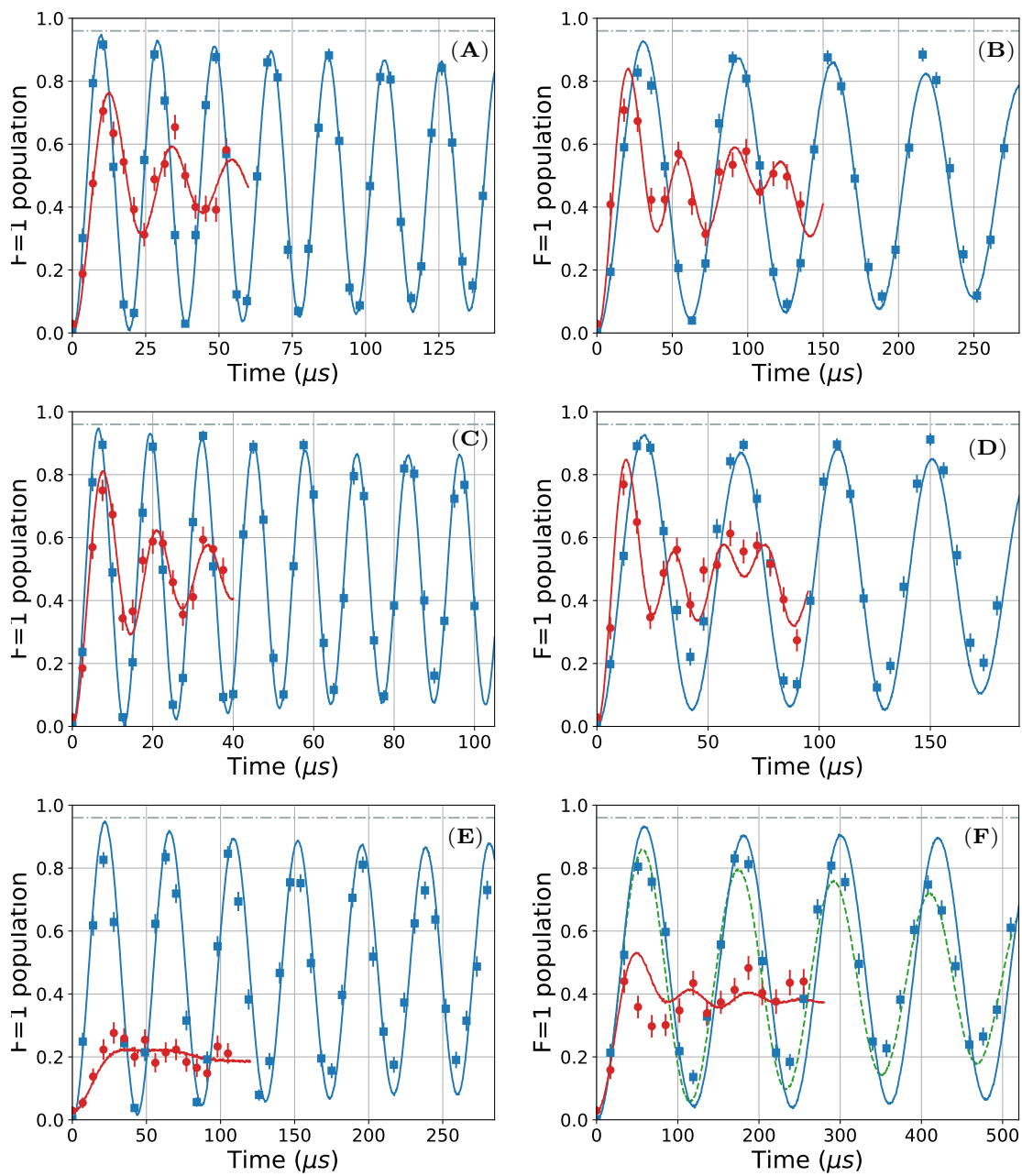
Figure 3.7 (following page): Rabi flopping on radial axis x (A) carrier and (B) $\Delta n_x = 1$ sideband, radial axis y (C) carrier and (D) $\Delta n_x = 1$ sideband, axial axis z (E) carrier and (F) $\Delta n_z = 1$ sideband, before (red circle) and after (blue square) Raman sideband cooling.

Solid lines (both red and blue) in all plots are fits to a Rabi-flopping that includes a thermal distribution of motional states as well as off-resonant scattering from the Raman beams.

The blue lines correspond to a ground state probability of (A-D) 98.1% along radial axis and (E-F) 95% along the axial axis after cooling. The red lines correspond to a thermal distribution of 80 μ K before RSC. The horizontal dashed lines in all the plots correspond to the 4 % probability of imaging loss.

The green dashed line in (F) includes the additional decoherence due to a fluctuation of the hyperfine splitting of magnitude 3 kHz. We see that the decoherence effect is strongest for the post-cooling data on the axial $\Delta n_z = 1$ sideband where the Rabi frequency is the lowest.

Figure 3.7: (continued)



4

Interaction of Single Atoms

4.1 SCATTERING LENGTH

(Importance/relation with binding energy etc.)

4.2 ENERGY LEVELS OF TWO INTERACTING ATOMS IN AN ANISOTROPIC TRAP

(appendix?)

4.3 INTERACTION SHIFT SPECTROSCOPY

(motional sideband, scattering length result)

4.4 SUMMARY AND OUTLOOK

(Motional state selection)

5

Photoassociation of Single Atoms

5.1 ENERGY LEVELS

5.2 EFFECT OF THE TRAP

(light shift, broadening)

5.3 PHOTOASSOCIATION SPECTROSCOPY

($v=0, 12, 14$, etc)

6

Two-photon Spectroscopy of NaCs

Ground State

6.1 INTRODUCTION

6.2 ENERGY LEVEL STRUCTURE FOR NaCs GROUND STATE

6.3 RAMAN RESONANCE ON $v'' = -1$, $N = 0$ GROUND STATE

6.4 RAMAN RESONANCE ON $v'' = -1$, $N = 2$ GROUND STATE

7

Coherent Optical Creation of NaCs

Molecule

7.1 INTRODUCTION

7.2 RAMAN TRANSFER EFFICIENCY MODEL

7.2.1 BEYOND THREE-LEVEL MODEL

7.2.2 DIFFERENTIAL LIGHT SHIFT

7.2.3 SCATTERING

7.2.4 RAMAN TRANSFER VERSUS STIRAP

7.3 EXCITED STATE SELECTION

7.4 GROUND STATES SELECTION

7.4.1 FINAL MOLECULAR STATE

7.4.2 INITIAL ATOMIC STATE

7.5 RAMAN TRANSITION RESULTS

7.5.1 SCALING OF RAMAN TRANSITION PARAMETERS

8

Conclusion



Computer Control Appendix

(Hardware spec)

B

Raman Sideband Cooling Appendix

Each Raman pulse in the cooling sequence is followed immediately by an optical pumping pulse.

The full parameters for the Raman pulses, including the cooling “axis”, the sideband “order (Δn)”, the cooling frequency “ δ' ”, the carrier ($\Delta n = 0$) frequency “ δ'_0 ”, the pulse “duration”, the pulse strength in “ Ω_0 ”, and the beam of which a non-uniform “power ramp” is applied, are listed in 6 groups below. The applied cooling frequency, δ' , is the two-photon detuning given relative to the

zero-field $F = 1$ and $F = 2$ hyperfine splitting of $1.7716261288(10)$ GHz^{Steck}. Due to the Stark shifts of the Raman beams, the carrier transition, δ'_0 , varies with the power of the Raman beams. δ'_0 is given also relative to the zero-field hyperfine splitting. The strength of the pulses given in Ω_0 determines the two-photon Rabi frequency, $\Omega_{n,\Delta n} = \Omega_0 \langle n | e^{i\vec{k}\cdot\vec{r}} | n + \Delta n \rangle$. We adopt the convention that a π -pulse between state n and $n + \Delta n$ requires a duration $\pi/\Omega_{n,\Delta n}$. The difference between δ' and δ'_0 gives the motional sideband frequency, δ . Many Raman pulses include a “power ramp” with a Blackman envelope^{Kasevich & Chu} to minimize off-resonant excitations. Because each Raman pulse is a product of two spatial- and temporal-overlapped laser beams, the “power ramp” is applied only to the beam that has the smaller light shift (we label the beam by the corresponding F number) while the other beam has a square-pulse shape. For a Raman pulse with a power ramp, the Rabi frequency gives the arithmetic mean over the duration of the pulse.

GROUP 1

This group is repeated 4 times.

Axis	Δn	δ' (MHz)	δ'_0 (MHz)	Duration (μs)	Ω_0 (kHz)	Power ramp
x	-2	19.625	18.649	44.1	$2\pi \times 23$	F ₁
y	-2	19.615	18.648	28.6	$2\pi \times 35$	F ₁
x	-1	19.130	18.649	36.9	$2\pi \times 23$	F ₁
y	-1	19.615	18.648	24.0	$2\pi \times 35$	F ₁

GROUP 2

This group is repeated 5 times.

Axis	Δn	δ' (MHz)	δ'_0 (MHz)	Duration (μs)	Ω_0 (kHz)	Power ramp
z	-5	19.030	18.605	81.5	$2\pi \times 16$	F ₂
x	-2	19.625	18.649	44.1	$2\pi \times 23$	F ₁
z	-4	18.940	18.605	76.3	$2\pi \times 16$	F ₂
y	-2	19.615	18.648	28.6	$2\pi \times 35$	F ₁
z	-5	19.030	18.605	81.5	$2\pi \times 16$	F ₂
x	-1	19.130	18.649	36.9	$2\pi \times 23$	F ₁
z	-4	18.940	18.605	76.3	$2\pi \times 16$	F ₂
y	-1	19.130	18.648	24.0	$2\pi \times 35$	F ₁

GROUP 3

This group is repeated 6 times.

Axis	Δn	δ' (MHz)	δ'_0 (MHz)	Duration (μs)	Ω_0 (kHz)	Power ramp
z	-4	18.940	18.605	76.3	$2\pi \times 16$	F ₂
x	-2	19.625	18.649	44.1	$2\pi \times 23$	F ₁
z	-3	18.858	18.605	70.2	$2\pi \times 16$	F ₂
y	-2	19.615	18.648	28.6	$2\pi \times 35$	F ₁
z	-4	18.940	18.605	76.3	$2\pi \times 16$	F ₂
x	-1	19.130	18.649	36.9	$2\pi \times 23$	F ₁
z	-3	18.858	18.605	70.2	$2\pi \times 16$	F ₂
y	-1	19.130	18.648	24.0	$2\pi \times 35$	F ₁

GROUP 4

This group is repeated 7 times.

Axis	Δn	δ' (MHz)	δ'_0 (MHz)	Duration (μs)	Ω_0 (kHz)	Power ramp
z	-3	18.858	18.605	70.2	$2\pi \times 16$	F ₂
x	-2	19.625	18.649	44.1	$2\pi \times 23$	F ₁
z	-2	18.773	18.605	62.7	$2\pi \times 16$	F ₂
y	-2	19.615	18.648	28.6	$2\pi \times 35$	F ₁
z	-3	18.858	18.605	70.2	$2\pi \times 16$	F ₂
x	-1	19.130	18.649	36.9	$2\pi \times 23$	F ₁
z	-2	18.773	18.605	62.7	$2\pi \times 16$	F ₂
y	-1	19.130	18.648	24.0	$2\pi \times 35$	F ₁

GROUP 5

This group is repeated 10 times.

Axis	Δn	δ' (MHz)	δ'_0 (MHz)	Duration (μ s)	Ω_0 (kHz)	Power ramp
z	-2	18.773	18.605	62.7	$2\pi \times 16$	F ₂
x	-1	19.130	18.649	36.9	$2\pi \times 23$	F ₁
z	-1	18.685	18.605	52.5	$2\pi \times 16$	F ₂
y	-1	19.130	18.648	24.0	$2\pi \times 35$	F ₁
z	-2	18.773	18.605	62.7	$2\pi \times 16$	F ₂
x	-1	19.130	18.649	70.0	$2\pi \times 23$	F ₁
z	-1	18.685	18.605	52.5	$2\pi \times 16$	F ₂
y	-1	19.130	18.648	46.0	$2\pi \times 35$	F ₁

GROUP 6

This group is repeated 30 times.

Axis	Δn	δ' (MHz)	δ'_0 (MHz)	Duration (μ s)	Ω_0 (kHz)	Power ramp
z	-1	18.683	18.605	78.7	$2\pi \times 11$	F ₂
z	-1	18.683	18.605	135.0	$2\pi \times 11$	F ₂
z	-1	18.685	18.605	78.7	$2\pi \times 11$	F ₂
x	-1	19.130	18.649	36.9	$2\pi \times 23$	F ₁
y	-1	19.130	18.648	24.0	$2\pi \times 35$	F ₁
z	-1	18.685	18.605	78.7	$2\pi \times 11$	F ₂
z	-1	18.685	18.605	135.0	$2\pi \times 11$	F ₂
z	-1	18.685	18.605	78.7	$2\pi \times 11$	F ₂
x	-1	19.130	18.649	70.0	$2\pi \times 23$	F ₁
y	-1	19.130	18.648	46.0	$2\pi \times 35$	F ₁

References

[Kasevich & Chu] Kasevich, M. & Chu, S. Laser cooling below a photon recoil with three-level atoms. 69(12), 1741–1744.

[Steck] Steck, D. A. Sodium d line data.